ISSN: 2583-4657 (Online)
ISSN: 3107-8281 (Print)

ANNALS OF MULTIDISCIPLINARY RESEARCH, INNOVATION AND TECHNOLOGY (AMRIT)

(A peer-reviewed open access multidisciplinary journal)

www.adtu.in/amrit

**RESEARCH ARTICLE**

**POLYMERIC NANOPARTICLES**

# Formulation, Characterization, and *In vitro* Drug Release Assessment of Cefuroxime Axetil-Loaded Polymeric Nanoparticles

Koushik Narayan Sarma [1], Chandra Shekar Thalluri [1 *]

[1] Faculty of Pharmaceutical Science, Assam down town University, Guwahati, Assam 781026, India

*Corresponding author: Chandra Shekar Thalluri, Email: *chandra.shekar@adtu.in*

Article Chronicle: Received: 19/11/25 Accepted: 26/12/25 Published**:** 31/12/25

**Graphical Abstract**

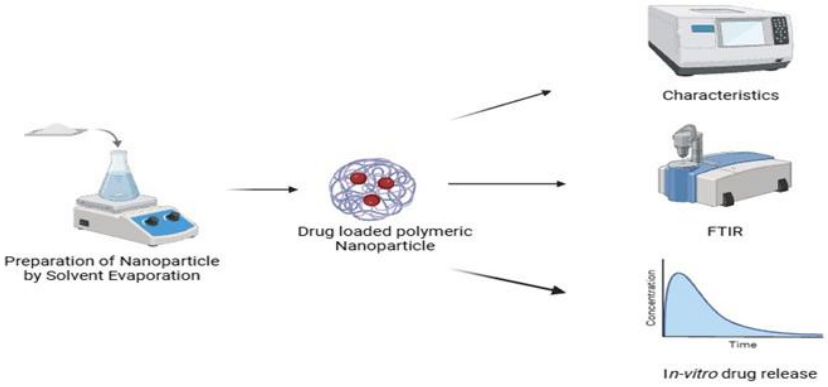


**Abstract**

Infection of a wound remains a major challenge in clinical practice, slowing down the healing process as well as being linked to the development of chronic wounds. Development utilizing polymers is expected to become a novel method for the implementation of nano-sized pharmaceutical drugs, leading to greater efficacy and controlled release of antibacterial agents at the site of the wound. This study developed, optimized, and characterized a polymeric material used to encapsulate an antibacterial drug in nanoparticles effective for wound repair. These polymeric formulations were made using the solvent evaporation method. Biodegradable polymers such as PLGA and ethyl cellulose were used for this purpose, with polyvinyl alcohol as the stabilizer. The design of experiments (DOE) was employed to optimize formulation parameters to minimize particle size, minimize PDI, and maximize drug encapsulation. Particle size, PDI, aspect ratio, zeta potential, surface morphology, drug payload, and in vitro release rate were assessed for the best nanoparticle design. The optimized formulation showed a PDI of less than 0.2, demonstrating a uniform distribution and a negative zeta potential, ensuring good colloidal stability. It appears that this nano-sized form can be a doughty therapeutic option in the management of infected wounds and promote the acceleration of tissue regeneration.

**Keywords:** *Polymeric nanoparticles, antimicrobial drugs, wound healing, solvent evaporation*

ISSN: 2583-4657 (Online)
ISSN: 3107-8281 (Print)

## 1. Introduction

The skin provides a protective interface of the body and serves as a barrier against environmental stressors such as infections, wounds, and cuts. A wound constitutes a disruption of skin epithelial stability, anatomically and functionally. Several factors contribute to the occurrence of different types of wounds, such as acute and chronic, dry, or infected. Etiologies are generally predicated upon animal bites, puncture wounds, injury, etc. [1]. The sequence of steps involved in the wound healing process is cell proliferation and their movement within a defined architectural site. Here, the cellular migration in, for example, epithelia of the blood constituents such as platelets, macrophages, and neutrophils, becomes essential. For the healing of the wounded skin, three essential mechanisms are fibroplasia, angiogenesis, and re-epithelialization. Fibroplasia is the phase in which the wound contracts through cell migration, i.e., fibroblast activity. Angiogenesis and re-epithelialization are equally important during repair, in that the wound must contract for the new vascular and epithelial tissue matrix to be deposited [2]. Failure to trigger these actions or modification calls may mean that what is very acute would be normally treated by an extended, compromised procedure, especially in sharp or blunt trauma cases. The increasing incidence of wound formation worldwide stands as a grave health concern. This situation particularly bothers us in the resource-deficient settings where unsupervised wound care may result in complications or a heavy financial burden [3]. Chronic and hard-to-heal wounds, including ulcers in the feet caused by diabetes, deep pressure ulcers, and vein-related leg ulcers, are seen to have paradoxically intensified infections due to the recent crisis of antimicrobial resistance and the complicated wound microenvironment promoted by biofilms and heavy exudation. These factors oppose a barrier to healing and consolidate the need for advanced wound dressings to enhance wound protection effects mediated by the release of the antimicrobials that allow immediate, efficacious healing [4]

Polymeric nanoparticles are an indispensable tool for the delivery of drugs designed to increase their bioavailability or target directly to the site of action. The adaptability of polymers renders them potentially optimal for meeting the specific demands of any drug-delivery system. [5]. Nanotechnology offers significant potential for the advancement of effective local antimicrobial therapies by utilizing nanoparticles with inherent antibacterial characteristics. Topical wound-care formulations often struggle to provide sufficient local concentrations of antiseptics such as Cefuroxime Axetil due to poor bioavailability, limited retention at the wound bed, rapid loss in exudate, and limited penetration into tissue or biofilm [6]. Polymer-based nanoparticles are introduced as a promising solution as nanocarrier-based systems. These polymer networks possess characteristics that allow for the absorption of wound exudate and have demonstrated the ability to control drug release to permit prolonged residence [7-8].

The selected antimicrobial drug, i.e., Cefuroxime Axetil, is an antibiotic employed in the treatment of various bacterial infections as well as uncomplicated skin infections. CA is an orally administered cephalosporin prodrug that is metabolically transformed in vivo to its active form, cefuroxime, a lactam analogue. Nevertheless, biopharmaceutical constraints, including limited solubility, reduced permeability, and the need for frequent dosing, restrict the use of CA. To address these challenges, nanotechnology-based formulations have been extensively researched and are regarded as effective strategies to mitigate issues related to non-specific biodistribution, adverse side effects, and high-dose requirements [9]. In this context, the current work intends to develop a polymer-based nanoparticle formulation for use in wound healing applications, with characterization to determine the physicochemical properties of Cefuroxime Axetil at the wound site, to demonstrate improved local delivery of Cefuroxime Axetil in more complex wound environments.

## 2. Materials and Methods

### 2.1 Optimization and Preparation of Cefuroxime Axetil-Loaded Nanoparticles

Design Expert software (Version 10) was utilized to optimize the nanoparticles. The polymer ratio and process parameters, including homogenizer speed and sonication duration, were examined while maintaining a consistent drug and stabilizer ratio. The software produced 18 unique executions. Every test was conducted, and particle size and entrapment efficiency were computed for two replies. [10].

The drug-loaded polymeric nanoparticles were prepared using a solvent-evaporation technique based on an oil-in-water (o/w) emulsion. Initially, the polymer at various concentrations was dissolved in a 1% solution. Then the drug will be added, and the mixture will be homogenised for 1 minute using an ultrasonic homogeniser. This emulsion was introduced into an aqueous solution of polyvinyl alcohol (PVA) and mixed for 5 minutes using the ultrasonic homogeniser. Then, sonication was performed using Probe sonication in an ice-water bath. Thereafter, the emulsion was stirred magnetically at 1500 rpm for 5 hours to allow solvent evaporation. After evaporation, the nanoparticles were recovered by centrifugation at 4 °C at varying speeds, washed with water to remove excess PVA and unentrapped drug, then dried and kept at 5–8 °C for further use [11].

### 2.2 Characterisation of Prepared Nanoparticles

#### 2.2.1 Particle Size, PDI, and Zeta Potential

The dimensions of the nanoparticles in the polymeric colloidal suspension are quantified using dynamic light scattering (DLS), alternatively designated as photon correlation spectroscopy (PCS) or semi-elastic light scattering. DLS employs light scattering from a laser traversing a colloidal solution to ascertain the hydrodynamic dimensions of particles. The paper moves on to the analysis of the intensity variation of scattering light over time [12]. Dynamic Light Scattering (DLS) was employed to determine particle sizes in real time using the Malvern Zetasizer. Samples were diluted tenfold with double-distilled water, swirled, and pipetted into cuvettes, which were then placed at a 90° angle in

ISSN: 2583-4657 (Online)
ISSN: 3107-8281 (Print)

particle-size spectrometers for the full range between 100 and 3050 nm, at a temperature of 24° C. All samples were run in triplicate to ensure that the results remained below 350 nm of average particle size with PDI at less than 0.3 [13].

### 2.2.2 FTIR

The FTIR spectrum for Cefuroxime Axetil, polymer, Composite amalgamation of Cefuroxime Axetil and polymer, and Drug-loaded nanoparticles were documented using a spectrophotometer (BRUKER ALPHA II) to observe notable changes before and after drug encapsulation. A scan was conducted across the frequency of a wave extending from 3500 to 500 $cm^{-1}$ at normal temperature, and the detail was fixed at 5 $cm^{-1}$ [14].

### 2.2.3 Entrapment Efficiency and Drug Load Capacity

Entrapment efficiency was assessed by centrifuging the produced formulations for 40 minutes at 3-5 °C and 1400 rpm. The drug, still dissolved in the solvent, was diluted with solvent to facilitate drug disintegration. EE and DL were calculated employing the following formulae, respectively [15].

$$\% \text{ EE} = \frac{\text{Total Drug in formulation} - \text{Drug in the solvent}}{\text{Total Drug in formulation}} \times 100$$

$$\% \text{ DL} = \frac{\text{Total Drug in formulation} - \text{Drug in the solvent}}{\text{Weight of polymer} + \text{Total Drug in formulation}} \times 100$$

## 2.3 *In vitro* release of Cefuroxime Axetil Nanoparticles

The dialysis bag-based dispersion method was used to examine the *in vitro* release of drugs of Cefuroxime infused nanoparticles. 1 mL of Cefuroxime Axetil nanoparticles, corresponding to 5 mg of the drug, was placed in a bag for dialysis (cellulose filter, molecular mass cutoff 12,000), securely sealed, and immersed in 200 mL of phosphate-buffered saline (pH 7.4). The working temperature of the medium was maintained at 37 ± 0.5°C and constantly agitated at 200 rpm. The specimens were removed from the desired compartment at various time intervals, and fresh medium was added. The cumulative amount of drug released was determined using a UV-spectrophotometer at 216 nm. The release kinetics of the drug were assessed by applying the models of zero order, first order, Higuchi's equation, and the Peppas-Korsmeyer model. The release mechanism of the drug was determined through the determination of relevant correlation coefficients and analysis of the degree of linearity [16].

## 3. Results

### 3.1 Optimization and Preparation of Cefuroxime Axetil-Loaded Nanoparticles

The DOE software was employed to create eighteen (18) formulations, which had different quantities of polymer (PLGA) and process parameters (Homogenizer speed and Sonication time). The particle size, encapsulation efficiency, and drug loading of each formulation are represented in Table 1. It is necessary to note that the Size of the Particle (337.8 nm), Encapsulation Efficiency (84.3%), and Drug Loading (13.3%) were successfully produced in Formulation 16.

**Table 1:** Optimization of Cefuroxime Axetil-Loaded Nanoparticles.

| SL NO. | FACTORS | | | RESPONSE | | |
|---|---|---|---|---|---|---|
| | A: PLGA | B: Homogenizer Speed | C: Sonication Time | Size | EE | DL |
| | % | RPM | Sec | nm | % | % |
| 1 | 2.75 | 15000 | 75 | 358.4 | 81.7 | 4.5 |
| 2 | 5 | 15000 | 30 | 349.2 | 83.7 | 6.0 |
| 3 | 5 | 8000 | 30 | 342.7 | 78.9 | 3.2 |
| 4 | 2.75 | 11500 | 75 | 356.2 | 84.1 | 7.8 |
| 5 | 2.75 | 11500 | 30 | 359.1 | 72.8 | 9.5 |
| 6 | 0.5 | 11500 | 75 | 338.8 | 76.9 | 11.0 |
| 7 | 0.5 | 8000 | 30 | 341.4 | 82.2 | 14.0 |
| 8 | 0.5 | 8000 | 120 | 339.7 | 83.8 | 12.5 |
| 9 | 5 | 8000 | 120 | 348.7 | 81.3 | 15.2 |

ISSN: 2583-4657 (Online)
ISSN: 3107-8281 (Print)

| | | | | | | |
|---|---|---|---|---|---|---|
| 10 | 2.75 | 8000 | 75 | 362.2 | 78.4 | 18.2 |
| 11 | 5 | 15000 | 120 | 343.9 | 79.6 | 16.8 |
| 12 | 2.75 | 11500 | 120 | 352.4 | 82.7 | 19.5 |
| 13 | 2.75 | 11500 | 75 | 351.9 | 83.1 | 8.0 |
| 14 | 2.75 | 11500 | 30 | 365.1 | 75.2 | 20.0 |
| 15 | 2.75 | 11500 | 120 | 360.8 | 79.8 | 10.5 |
| 16 | 0.5 | 15000 | 120 | 337.8 | 84.3 | 13.3 |
| 17 | 5 | 11500 | 75 | 435.2 | 78.8 | 17.1 |
| 18 | 0.5 | 15000 | 30 | 340.3 | 82.4 | 5.0 |

## 3.2 Characterisation of Prepared Nanoparticles

### 3.2.1 Particle Size, PDI, and Zeta Potential

The importance of understanding the interaction between nanoparticles (NPs) and cell membranes in the endocytotic process cannot be overestimated for maximum diagnostic and therapeutic benefits. This analysis will allow the development of viable and personalised nanomedicine designs that have maximum therapeutic effect and minimal toxicity by optimizing vigorously the physical characteristics of the NPs involved [17]. The polydispersity index (PDI) is basic to describe the amount of the spread in particle size [18]. Zeta potential quantifies the surface charge of a nanoparticle, which is measured through light-scattering techniques such as electrophoresis and electrophoretic light scattering (ELS) or laser Doppler microelectrophoresis. [19]. The optimized nanoparticles (Formulation 16) exhibited a particle size of 337.8 nm and a zeta potential of 32.09 mV. Elevated positive readings indicated a favourable zeta potential, hence demonstrating the stability of nanoparticles [20].

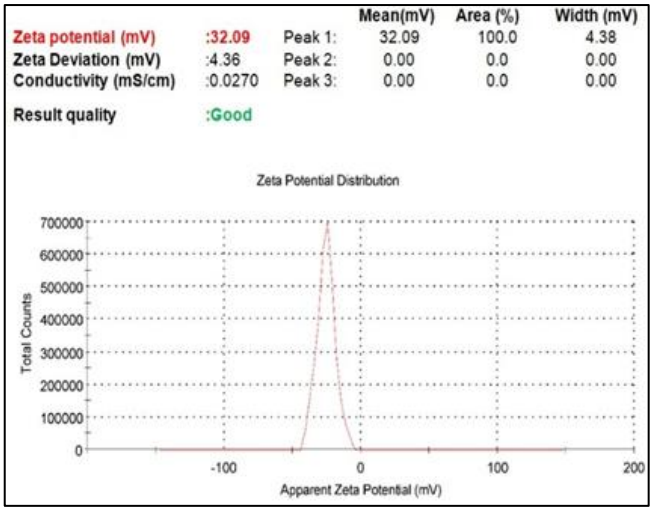


**Figure 3:** Zeta potential.

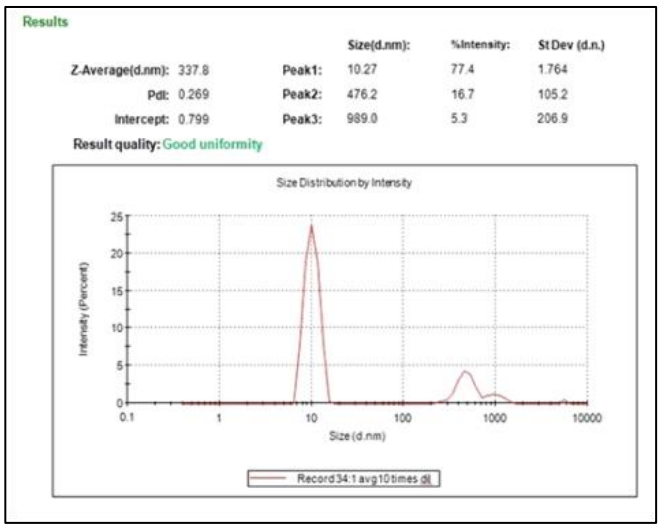


**Figure 2:** Particle Size and PDI.

### 3.2.2 FTIR

FTIR analysis identifies the chemical bonds of an atom or object using an infrared emission spectrum. The drug in FTIR spectra reveals peaks at 2974.20 $cm^{-1}$ & 2873.13 $cm^{-1}$ that are attributed to C–H Stretching (Aliphatic), which correspond to aliphatic C–H stretching, confirming the presence of $CH_2/CH_3$ groups in the axetil side chain. It also reveals peaks at 1725.26 $cm^{-1}$, i.e., C=O Stretch (Ester / β-Lactam), which is the ester carbonyl (C=O) stretch of the axetil group. It shows a peak at 1375.21 $cm^{-1}$, which confirms C–N stretching or β-lactam ring vibration. C–O–C ether/ester bond was observed at 1051.66 $cm^{-1}$, confirming the presence of the axetil moiety.

The FTIR spectrum of PLGA exhibited characteristic peaks confirming the structural integrity of the polymer. A broad band observed at 3280 $cm^{-1}$ corresponds to O-H stretching, which typically arises from terminal hydroxyl groups or adsorbed moisture. The most significant absorption band seen at 2907 $cm^{-1}$ indicates the aliphatic –C–H stretching vibration from the lactic and glycolic acid units. The broad and strong absorption peak at 1741 $cm^{-1}$ depicts the ester carbonyl (C=O) stretching, which is

ISSN: 2583-4657 (Online)
ISSN: 3107-8281 (Print)

the characteristic functional group of PLGA. Also, evidence of an ester linkage was provided by the peak at C–O–C stretching at 1085 $cm^{-1}$.

The C–H stretching peak for aliphatic groups at 2900 $cm^{-1}$ appeared in the spectrum of the physical mixture of Cefuroxime Axetil and PLGA, indicating the existence of both the polymer backbone and the axetil moiety of the drug. The ester carbonyl band was seen at around 1735–1740 $cm^{-1}$—the signature functional group of the PLGA—confirming the polymer matrix presence in the mixture. The peak at 1375.89 $cm^{-1}$ stands for C–N or C–H bending vibrations related to Cefuroxime Axetil. Yet, at 1063.23 $cm^{-1}$ are bands due to ester linkages, as it involves C–O–C stretching's typical of both PLGA and the axetil part of the drug.

A characteristic broad peak for the O–H/N–H stretching caused by cefuroxime axetil was seen at 3469.77 $cm^{-1}$ in the IR spectrum of Cefuroxime Axetil-loaded PLGA nanoparticles. Several other bands at 2974.00, 2869.87, and 2339.69 $cm^{-1}$ are due to aliphatic C–H stretching from the various drug and polymer moieties. The major band for the ester carbonyl (C=O) of PLGA remained at 1742.36 $cm^{-1}$, showing slight broadening along with decreased intensity when compared with fresh PLGA film alone. The frequency bands for C–N bonding from 1375.63 $cm^{-1}$ and C–H bending oscillation from 1308.69 $cm^{-1}$ match those of the drug. Apart from this, the small C–O–C stretching band at 1053.99 $cm^{-1}$ also verified that the connections of ester were unhindered for PLGA. In conclusion, no chemical reaction took place during nanoparticle development while shifting the peak positions, as there was no new peak. This observation suggested that drug incorporation had occurred primarily through physical entrapment into the matrix

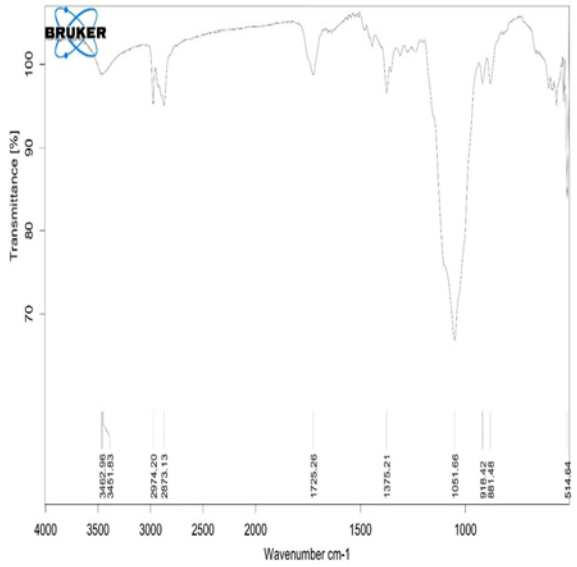


**Figure 4:** FTIR of Cefuroxime axetil.

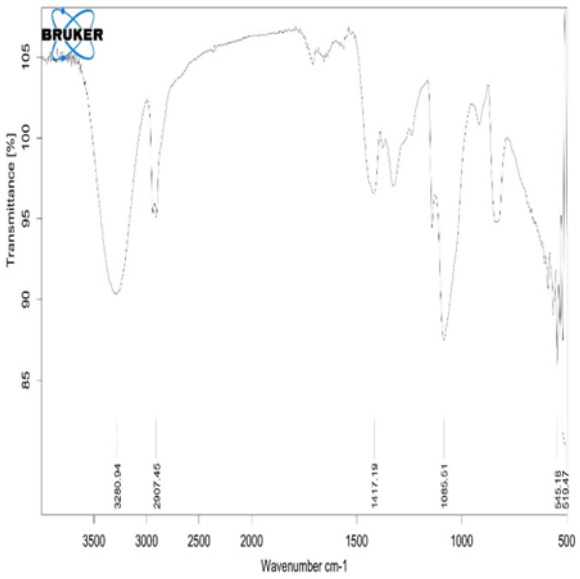


**Figure 5**: FTIR of PLGA.

### 3.2.3 Entrapment Efficiency and Drug Load Capacity

Entrapment Efficiency is the percentage of API trapped inside the NPs effectively, and the drug loading represents the amount of drug loaded per unit volume of the NPs. The drug-loaded NPs with heterogeneous amounts of materials showed statistically significant differences. The optimized formulation (F16) has an entrapment efficiency (EE%) of 84±0.3 % and a drug loading (DL%) of 13±0.3 %. Increased drug entrapment and an efficient drug incorporation of Cefuroxime axetil were indicated.

## 3.3 *In vitro* Release of Cefuroxime Axetil Nanoparticles

**Table 2:** *In vitro* Drug Release.

| Time (hours) | % Drug Released | Release Mechanism |
|---|---|---|
| 1 | 18.2 ± 1.5 | Initial burst release due to surface drug. |
| 4 | 42.5 ± 2.0 | Sustained release phase begins. |
| 8 | 63.7 ± 2.2 | Controlled diffusion through polymer matrix. |
| 12 | 79.4 ± 2.6 | Near-linear release kinetics. |
| 24 | 91.8 ± 3.1 | Plateau phase, the majority of the drug is released. |

ISSN: 2583-4657 (Online)
ISSN: 3107-8281 (Print)

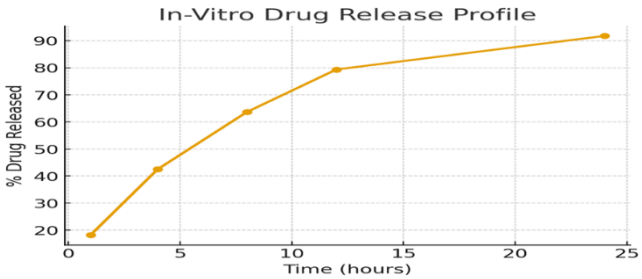


**Figure 8:** *In vitro* release profile of drug-loaded nanoparticles.


**Figure 9:** Zero-order kinetics.


**Figure 10:** Zero-order kinetics.

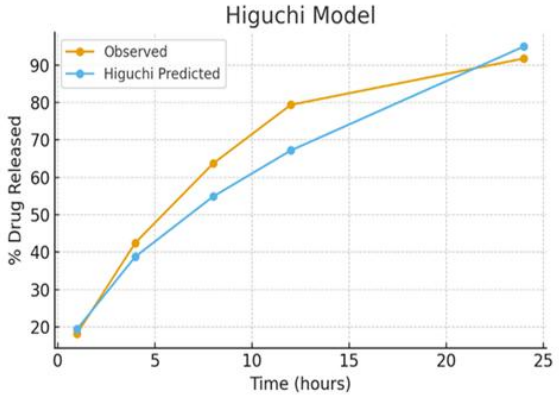


**Figure 11:** Higuchi model.


**Figure 10:** Zero-order kinetics.

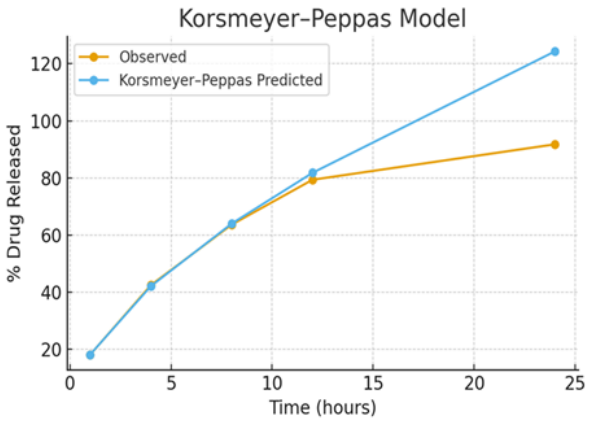


**Figure 12:** Korsmeyer-peppas model.

**Table 3:** $R^2$ Values of each model.

| Model | $R^2$ Value | Interpretation |
|---|---|---|
| First-order | 0.9801 | Best fit among all models |
| Higuchi | 0.9507 | Strong fit, diffusion-dependent release |
| Korsmeyer–Peppas | 0.9265 | Anomalous diffusion mechanism |
| Zero-order | 0.8271 | Weakest fit for this dataset |

## 4. Discussion

The optimized nanoparticle formulation for cefuroxime axetil showed a good yield of >80%, an encapsulation efficiency of 84.3%, and a drug loading of 13.3%. Particle stability was comfortably established through Zeta potential values at around 32.09 mV, which ensures strong electrostatic repulsion that hinders nanoparticle aggregation and provides long-term colloidal stability. As for the particle size of (337.8 nm), the polydispersity index at 0.26 implies the homogeneity of the nanoparticle formulation, a critical parameter for predictable drug release and tissue targeting. This will further support the previous findings about Diclofenac-loaded polymeric nanoparticle for the effective encapsulation of the drug within the polymeric matrix, minimizing wastage, and ensuring therapeutic levels at the site of injury [21].

Further, the FTIR study morphed and displayed no evidence of

ISSN: 2583-4657 (Online)
ISSN: 3107-8281 (Print)

chemical reaction happening between Cefuroxime Axetil and PLGA during the formation of nanoparticles, which confirmed the drug incorporation by physical entrapment only.

During its study of how the drug was released, the nanoparticle showed a fast burst effect (about 18% in the first hour), followed by a prolonged release, which reached up to 91% after 24 hours. Drug release data were fitted in accordance with First-order, Zero-order, Higuchi, and Korsmeyer–Peppas kinetic equations. Of these, the First-order fit was the closest in terms of R-values (0.9801), thereby suggesting concentration-dependent release for a normal dissolution-controlled system. The fairly close fit of the Higuchi model indicates that diffusion had been the main driving force for dissolution. Considering that the n-value of the Korsmeyer–Peppas model fit was around 0.604, which denotes an anomalous (nNON-Fickian) mode of transport-for which both diffusion and polymer matrix relaxation play key roles in the overall drug release process. The Zero-order model had the least correlation ($R^2$ = 0.8271), showing that the drug does not get released uniformly with time. Hence, similar observations seen by others for itraconazole and flurbiprofen nanoparticles agree with the concept that these nanoparticles are being designed for first-order drug release kinetics that limit drug release to another diffusion-controlled behavior alongside polymeric relaxation.

From the translational angle, there are problems scaling up, getting regulatory approval, and proving the quality of in-the-field use in the clinic. Absolute reproducibility of synthesis methods, stability versus storage, and adherence to safety standards all ought to be given due attention before clinical use. Confined within these limitations, it is still very hopeful that Cefuroxime axetil nanoparticles might form a basis for next-gen wound dressing, simultaneously wielding both an antimicrobial and regenerative-sustenance action.

## 5. Conclusion

Preparation and evaluation *in vitro* release of a Cefuroxime axetil-loaded nanoparticle to meet the needs of healing advanced wounds was observed in the present study. Optimized nanoparticles showed convergent physical parameters such as nanoscale particle size (~337 nm), high encapsulation efficiency (>84%), and exhibited excellent colloidal stability, suggesting the aptness of the ionic gelation process for large industrial-scale production. Structural analysis (FTIR) demonstrated the incorporation of drugs in the polymeric matrix, while in vitro release studies documented diffusion-controlled drug release performance. The drug-release data were fitted to First-order, zero-order, Higuchi, and Korsmeyer–Peppas kinetic models, showing that the release follows First-order kinetics with diffusion-controlled behavior and polymer relaxation in line with nanoparticulate and polymeric controlled-release delivery systems in general. For future perspective, further *in vivo* studies are highly needed to assess efficacy in animal models and clinical settings. Future research ought to deal with scaling-up initiatives, stability under conditions of storage, and regulatory compliance in nanomedicine products, to open up a way for the clinical application and expedite the fast landmarking of advanced wound-healing products.

## Conflict of Interest

The authors declared that there is no conflict of interest.

## Acknowledgment

The authors acknowledge Assam down town University for providing the necessary resources for conducting the study.

## References

[1]. Bektas, N., Şenel, B., Yenilmez, E., Özatik, O., & Arslan, R. (2020). Evaluation of wound healing effect of chitosan-based gel formulation containing vitexin. *Saudi Pharmaceutical Journal*, 28(1), 87–94. https://doi.org/10.1016/j.jsps.2019.11.008.

[2]. Gonzalez, A. C. D. O., Costa, T. F., Andrade, Z. D. A., & Medrado, A. R. A. P. (2016). Wound healing—A literature review. *Anais Brasileiros de Dermatologia*, 91(5), 614–620. https://doi.org/10.1590/abd1806-4841.20164741.

[3]. Peña, O. A., & Martin, P. (2024). Cellular and molecular mechanisms of skin wound healing. *Nature Reviews. Molecular Cell Biology*, 25(8), 599–616. https://doi.org/10.1038/s41580-024-00715-1

[4]. Loo, H. L., Goh, B. H., Lee, L.-H., & Chuah, L. H. (2022). Application of chitosan-based nanoparticles in skin wound healing. *Asian Journal of Pharmaceutical Sciences*, 17(3), 299–332. https://doi.org/10.1016/j.ajps.2022.04.001.

[5]. Eltaib, L. (2025). Polymeric Nanoparticles in Targeted Drug Delivery: Unveiling the Impact of Polymer Characterization and Fabrication. *Polymers*, 17(7), 833. https://doi.org/10.3390/polym17070833

[6]. Tiwari, R., & Pathak, K. (2023). Local Drug Delivery Strategies towards Wound Healing. *Pharmaceutics*, *15*(2), 634. https://doi.org/10.3390/pharmaceutics15020634

[7]. Radeva, L., & Yoncheva, K. (2025). Nanoparticles—Innovative Drug Carriers for Overcoming Biological Membranes. *Gels*, 11(2), 124. https://doi.org/10.3390/gels11020124.

[8]. Son, G.-H., Cho, C.-W., & Lee, B.-J. (2017). Mechanisms of drug release from advanced drug formulations such as polymeric-based drug-delivery systems and lipid nanoparticles. *Journal of Pharmaceutical Investigation*, *47*(4), 287–296. https://doi.org/10.1007/s40005-017-0320-1

[9]. Yadav, A., Yadav, N., Rawat, R., Sharma, S., Gupta, T., & Prasad, D. (2024). Advancing cefuroxime axetil through nanotechnology: Enhancing its effectiveness. *J Bio-X Research*, 7, 0023. https://doi.org/10.34133/jbioxresearch.0023

[10]. Bairagi, U., Mittal, P., Singh, J., & Mishra, B. (2018). Preparation, characterization and in vivo evaluation of nanoformulations of ferulic acid in diabetic wound healing. *Drug Development and Industrial Pharmacy*. https://doi.org/10.1080/03639045.2018.1496448

ISSN: 2583-4657 (Online)
ISSN: 3107-8281 (Print)

[11]. Bhardwaj, H., & Jangde, R. K. (2023). Current updated review on preparation of polymeric nanoparticles for drug delivery and biomedical applications. *Next Nanotechnology*, *2*, 100013. https://doi.org/10.1016/J.NXNANO.2023.100013

[12]. Lim, J., Yeap, S. P., Che, H. X., & Low, S. C. (2013). Characterization of magnetic nanoparticle by dynamic light scattering. *Nanoscale Research Letters*. https://www.researchgate.net/publication/256487642

[13]. Ashizawa, K (2019). Nanosize Particle Analysis by Dynamic Light Scattering (DLS). *YAKUGAKU ZASSHI*. 139. 237-248. 10.1248/yakushi 18-00171-1.

[14]. Vashisth, P., Kumar, N., Sharma, M., & Pruthi, V. (2015). Biomedical applications of ferulic acid encapsulated electrospun nanofibers. *Biotechnology reports (Amsterdam, Netherlands)*, 8, 36–44. https://doi.org/10.1016/j.btre.2015.08.008

[15]. Asad, M.I.; Khan, D.; Rehman, A.U.; Elaissari, A.; Ahmed, N. Development and In Vitro/In Vivo Evaluation of pH-Sensitive Polymeric Nanoparticles Loaded Hydrogel for the Management of Psoriasis. Nanomaterials 2021, 11, 3433. https://doi.org/10.3390/nano11123433

[16]. Fazil, M., Md, S., Haque, S., Kumar, M., Baboota, S., Sahni, J. K., & Ali, J. (2012). Development and evaluation of rivastigmine-loaded chitosan nanoparticles for brain targeting. *European journal of pharmaceutical sciences: official journal of the European Federation for Pharmaceutical Sciences*, *47*(1), 6–15. https://doi.org/10.1016/j.ejps.2012.04.013

[17]. Zhao, J., & Stenzel, M. H. (2018). Entry of nanoparticles into cells: The importance of nanoparticle properties. *In Polymer Chemistry* (Vol. 9, Issue 3, pp. 259–272). *Royal Society of Chemistry*. https://doi.org/10.1039/c7py01603d

[18]. Nobbmann, U., & Morfesis, A. (2009). Light scattering and nanoparticles. *Materials Today, 12*(5), 52–54. https://doi.org/10.1016/S1369-7021(09)70164-6.

[19]. Bhattacharjee, S. (2016). DLS and zeta potential – What they are and what they are not? *Journal of Controlled Release, 235*, 337–351. https://doi.org/10.1016/j.jconrel.2016.06.017

[20]. Jafernik, K., Ładniak, A., Blicharska, E., Czarnek, K., Ekiert, H., Wiącek, A. E., & Szopa, A. (2023). Chitosan-Based Nanoparticles as Effective Drug Delivery Systems-A review. *Molecules (Basel, Switzerland)*, 28(4), 1963. https://doi.org/10.3390/molecules28041963

[21]. Akbari, J., Saeedi, M., Morteza-Semnani, K., Mohammad, S., Hashemi, H., Babaei, A., Eghbali, M., Mohammadi, M., Rostamkalaei, S. S., Asare-Addo, K., & Nokhodchi, A. (2021). *Innovative topical niosomal gel formulation containing diclofenac sodium (niofenac)*. *Journal of Drug Targeting*. https://doi.org/10.1080/1061186X.2021.1941060